

THE DIVERSE HOT GAS CONTENT AND DYNAMICS OF OPTICALLY SIMILAR LOW-MASS ELLIPTICAL GALAXIES

ÁKOS BOGDÁN^{1,2}, LAURENCE P. DAVID¹, CHRISTINE JONES¹, WILLIAM R. FORMAN¹, AND RALPH P. KRAFT¹

¹Smithsonian Astrophysical Observatory, 60 Garden Street, Cambridge, MA 02138, USA

Draft version March 7, 2019

ABSTRACT

The presence of warm X-ray emitting gas is nearly ubiquitous in massive early-type galaxies. However, much less is known about the X-ray gas content and physical status of the warm gas in low-mass ellipticals. In the present paper we study the X-ray gas content of four low-mass elliptical galaxies using archival *Chandra* X-ray observations. The sample galaxies, NGC821, NGC3379, NGC4278, and NGC4697, have approximately identical K-band luminosities, and hence stellar masses, yet their X-ray appearance is strikingly different. We conclude that the unresolved emission in NGC821 and NGC3379 is built up from the multitude of faint compact objects, such as coronally active binaries (ABs) and cataclysmic variables (CVs). Despite the non-detection of warm X-ray gas, these galaxies may host low density, hence low luminosity X-ray gas components, which undergo an SN Ia driven outflow. We detect warm X-ray gas with temperature of $kT \sim 0.6$ keV in the central $\sim 35''$ (~ 2.8 kpc) region of NGC4278. We demonstrate that the X-ray gas exhibits a bipolar morphology in the northeast-southwest direction, indicating that the X-ray gas may be outflowing from the galaxy. The mass and energy budget of the outflow can be maintained by evolved stars and Type Ia Supernovae (SNe Ia), respectively. The X-ray gas in NGC4697 has an average temperature of $kT \sim 0.3 - 0.4$ keV, and has a significantly broader distribution than the stellar light. From the parameters of the warm X-ray gas, we conclude that the gas in NGC4697 is most likely in hydrostatic equilibrium, although a subsonic outflow may be present.

Subject headings: galaxies: elliptical and lenticular, cD — galaxies: individual (NGC821, NGC3379, NGC4278, NGC4697) — galaxies: ISM — X-rays: galaxies — X-rays: general — X-rays: ISM

1. INTRODUCTION

Although the warm X-ray emitting gas content of massive ($M_\star > 10^{11} M_\odot$) elliptical galaxies has been studied in full particulars (e.g. Forman et al. 1985; Mathews & Brighenti 2003; Randall et al. 2006; Forman et al. 2007; Kraft et al. 2011), the X-ray gas content of low-mass ellipticals is less explored. The major issue in studying low-mass ellipticals ($M < 10^{11} M_\odot$) is their relatively X-ray faint nature. In particular, the observed X-ray emission from low-mass elliptical galaxies is dominated by the population of resolved and unresolved compact X-ray sources. Besides the population of compact objects, emission from warm X-ray gas may also be present, whose detection may be compromised by the underlying emission from unresolved compact objects. Moreover, given the shallow potential well of such galaxies, the warm X-ray emitting gas may not be in a stationary state. SNe Ia might be energetically capable of driving galactic-scale outflows (David et al. 2006). In agreement with this result, a galactic-scale outflow had been detected in the bulge of M31 (Li & Wang 2007; Bogdán & Gilfanov 2008) and in the Sombrero galaxy (Li et al. 2011).

Detailed X-ray studies of the Milky Way and nearby galaxies have led to a better understanding of the origin of resolved and unresolved X-ray emission. With the superior angular resolution of *Chandra*, the population of bright low-mass X-ray binaries (LMXBs) could be stud-

ied in full particulars (e.g. Gilfanov 2004). Moreover, it has been established that (at least) a portion of unresolved X-ray emission is associated with the stellar population and is the superposition of a multitude of faint compact sources, such as ABs and CVs (Sazonov et al. 2006; Revnivtsev et al. 2006, 2009). Thus, if sufficiently deep *Chandra* observations are available, the various X-ray emitting components can be identified in nearby galaxies, hence the diffuse emission from warm X-ray gas can be separated from the population of resolved and faint unresolved compact objects. This extensive knowledge permits us to determine whether low-mass ellipticals host warm X-ray emitting gas, and additionally, address the state of the warm gas.

In the present paper we study four elliptical galaxies, whose optical appearances are nearly identical, yet their X-ray properties are strikingly different. The four galaxies, NGC821, NGC3379, NGC4278, and NGC4697, are relatively nearby ($D = 9.8 - 24.1$ Mpc), and have deep *Chandra* observations (Figure 1). Therefore, we are able to identify and remove the bulk of the X-ray emission from LMXBs, hence bright point sources do not significantly contaminate the diffuse emission. Furthermore, the low and stable instrumental background of *Chandra* permits us to reliably study low surface brightness emission. The goals of this paper are twofold: First, we aim to unveil whether the sample galaxies host a significant amount of warm X-ray emitting gas. Second, if they do possess X-ray gas, we intend to measure its properties, morphology, and understand its physical state.

E-mail: abogdan@cfa.harvard.edu

²Einstein Fellow

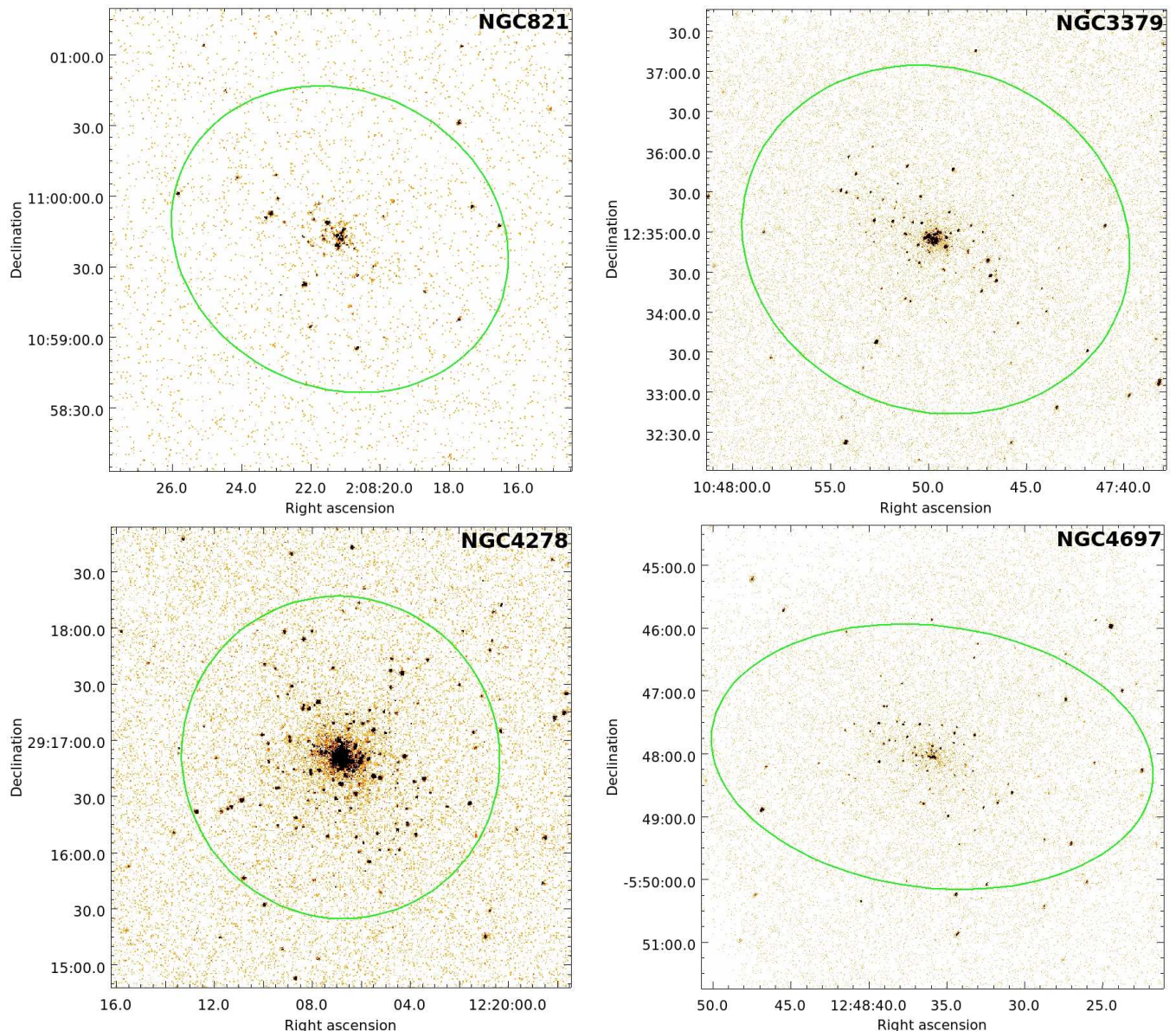


FIG. 1.— 0.5 – 2 keV band unprocessed *Chandra* images of the four analyzed galaxies. Majority of the bright point sources are low-mass X-ray binaries associated with the galaxies, minor fraction of them are background AGN. The overplotted elliptic regions show the D_{25} ellipses, whose extent are listed in Table 1.

The resolved and unresolved X-ray emitting components of NGC821 have been studied by Pellegrini et al. (2007) using *Chandra* X-ray observations. Besides the thorough analysis of bright LMXBs, they also concluded that the bulk of the unresolved emission originates from unresolved LMXBs and warm X-ray gas may only be present in the inner $10''$ region. The unresolved X-ray emission of NGC3379 was first investigated by David et al. (2005), based on a 32 ks *Chandra* observation. They concluded that warm X-ray gas may be present within the central $15''$ region with a temperature of $kT = 0.6$ keV. Based on a much deeper, 341 ks, *Chandra* data set, Revnivtsev et al. (2008) claimed that NGC3379 is virtually gas free, and the unresolved X-ray emission is built up from faint undetected compact objects, mostly by ABs and CVs. However, based

on the same data set, Trinchieri et al. (2008) reported that NGC3379 hosts warm X-ray gas in the central $15''$ region, which is outflowing from the galaxy. Although the population of resolved sources in NGC4278 has been extensively studied (e.g. Kim et al. 2006), the unresolved emission from NGC4278 has not been investigated in full particulars. The unresolved X-ray emitting components of NGC4697 were explored by Sarazin et al. (2001) based on a 40 ks *Chandra* observation. They demonstrated the presence of warm X-ray gas, which has a significantly broader distribution than the stellar light. However, more recently NGC4697 was observed by *Chandra* for an additional ~ 150 ks, which may offer a better understanding of the properties and physical state of its warm X-ray gas. Although, the X-ray emitting components of the sample galaxies were discussed by a number of

TABLE 1
ELLIPTICAL GALAXIES STUDIED IN THIS PAPER.

Name	Distance (Mpc)	L_K ($L_{K,\odot}$)	M_*/L_K ($M_\odot/L_{K,\odot}$)	M_* (M_\odot)	N_H (cm^{-2})	Morph. type	T_{obs} (ks)	T_{filt} (ks)	L_{lim} (erg s^{-1})	D_{25} ($2a, 2b, \theta$)
	(1)	(2)	(3)	(4)	(5)	(6)	(7)	(8)	(9)	(10)
NGC821	24.1 ^a	8.2×10^{10}	0.83	6.8×10^{10}	6.4×10^{20}	E6	229.7	187.6	2×10^{37}	2.45', 2.10', 26.0°
NGC3379	9.8 ^b	6.1×10^{10}	0.83	5.1×10^{10}	2.9×10^{20}	E1	341.4	310.0	2×10^{36}	4.90', 4.27', 71.0°
NGC4278	16.1 ^a	7.1×10^{10}	0.82	5.8×10^{10}	1.8×10^{20}	E1-2	476.7	437.5	4×10^{36}	2.88', 2.82', 27.5°
NGC4697	11.8 ^a	8.1×10^{10}	0.82	6.6×10^{10}	2.1×10^{20}	E6	195.7	159.9	5×10^{36}	7.08', 4.17', 83.1°

Note. Columns are as follows. (1) References are: ^a Tonry et al. (2001) – ^b Jensen et al. (2003). (2) Total K-band luminosity. (3) K-band mass-to-light ratios computed from Bell et al. (2003) using the $B - V$ color indices of galaxies (de Vaucouleurs et al. 1991). (4) Total stellar mass based on the K-band luminosity and the K-band mass-to-light ratios. (5) Galactic absorption (Dickey & Lockman 1990). (6) Morphological type, taken from NED (<http://nedwww.ipac.caltech.edu/>). (7) and (8) *Chandra* exposure times before and after flare filtering. (9) Source detection sensitivity in the 0.5 – 8 keV energy range. (10) Major axis diameter, minor axis diameter, and position angle of the D_{25} ellipse.

authors, these works often use different analysis methods and techniques, which may lead to different conclusions. Moreover, accurate calibration of the population of faint compact objects only became available relatively recently. Hence in some of the previous works, the emission from these sources could not be precisely disentangled from the warm X-ray gas. Therefore, our uniform analysis of the sample galaxies with the most up-to-date calibration of LMXBs and faint compact objects can lead to a better understanding of the warm X-ray gas content of low-mass ellipticals.

The paper is structured as follows: In Section 2, we introduce the analyzed galaxy sample. In Section 3, we describe the reduction of the data. In Section 4, we study the properties of the warm gas content of the sample galaxies. The physical state of the detected warm X-ray gas is discussed in Section 5, and we summarize our results in Section 6.

2. SAMPLE SELECTION

To identify the most suitable galaxies for our analysis, we rely on the volume limited ATLAS^{3D} catalog, which consists of 260 nearby early-type galaxies (Cappellari et al. 2011). To study low-mass ellipticals that may host a notable amount of warm X-ray gas, we selected galaxies with $M_K > -24$ mag ($L_K < 8.2 \times 10^{10} L_{K,\odot}$) and with morphological types $T < -1.5$. Finally, we filtered galaxies by distance and selected those with distances $D < 30$ Mpc. The obtained list includes a sample of 41 galaxies.

In order to study the unresolved emission and unveil the presence of a possible warm X-ray gas component, the bulk of the luminosity from LMXBs must be removed. Therefore, we demand a minimum source detection sensitivity of $\sim 3 \times 10^{37} \text{ erg s}^{-1}$, which assures that at least $\sim 75\%$ of the luminosity from LMXBs can be subtracted (Gilfanov 2004). To identify galaxies with sufficiently deep *Chandra* exposures, the list of 41 galaxies from the ATLAS^{3D} catalog was cross-correlated with the *Chandra* archive. We find that four nearby low-mass elliptical galaxies have deep enough *Chandra* data to resolve sources with luminosities exceeding $3 \times 10^{37} \text{ erg s}^{-1}$. These four galaxies are NGC821, NGC3379, NGC4278, and NGC4697. Basic properties of the sample galaxies are listed in Table 1.

The remaining sample of 37 low-mass elliptical galaxies, identified in the ATLAS^{3D} catalog, have source de-

tection sensitivities of $> 3 \times 10^{37} \text{ erg s}^{-1}$. Their warm X-ray gas content and the physical state of the X-ray gas will be discussed in a forthcoming study (L. David et al. in preparation).

3. DATA REDUCTION

3.1. *Chandra*

To study the various X-ray emitting components of the sample galaxies, we rely on *Chandra* observations. The list of analyzed observations is given in Table 2. To reduce the data, we use the standard CIAO software package tools¹ (CIAO version 4.3; CALDB version 4.4.2).

As a first step of the data preparation, we filter the flare contaminated time intervals for each observation, following the method described in Bogdán & Gilfanov (2008). On average, the clean exposure times are $\sim 10 - 15\%$ shorter than the original exposures (Table 2). For each galaxy, the flare-filtered observations were combined and merged to the coordinate system of the observation with the longest exposure time.

To detect point sources, we use the CIAO WAVDETECT tool on the merged unfiltered data set in the 0.5 – 8 keV energy range. As our particular aim is to study the diffuse emission, we changed the values of several parameters to obtain larger source cells – for a detailed description see Bogdán & Gilfanov (2008). Since NGC3379 and NGC4278 host ultraluminous X-ray sources at their centers, spill-over counts from these sources could add a notable contribution to the unresolved emission. To avoid this problem, we excluded the central 7'' and 5'' radius regions of NGC3379 and NGC4278. We note that for point source detection we used the original unfiltered data set, since the longer exposures outweigh the high background periods, thereby resulting in a better source detection sensitivity. The lists of detected sources were used to mask out the point sources for further study of the diffuse emission. To correct for vignetting and to estimate source detection sensitivities, exposure maps were produced using a power law model with a slope of $\Gamma = 1.56$, typical for LMXBs (Irwin et al. 2003). Assuming this spectrum, we also estimated the source detection sensitivity of the combined observations, which for all four galaxies is better than $\sim 3 \times 10^{37} \text{ erg s}^{-1}$.

¹ <http://cxc.harvard.edu/ciao/>

TABLE 2
THE LIST OF ANALYZED *Chandra* OBSERVATIONS.

Galaxy	Obs ID	T_{obs} (ks)	T_{filt} (ks)	Instrument
NGC821	4006	13.7	9.5	ACIS-S
NGC821	4408	25.3	5.5	ACIS-S
NGC821	5691	40.1	35.9	ACIS-S
NGC821	5692	28.0	24.6	ACIS-S
NGC821	6310	32.4	29.3	ACIS-S
NGC821	6313 [†]	50.1	46.7	ACIS-S
NGC821	6314	40.1	36.1	ACIS-S
NGC3379	1587	31.9	24.8	ACIS-S
NGC3379	7073 [†]	85.2	75.8	ACIS-S
NGC3379	7074	70.0	65.5	ACIS-S
NGC3379	7075	84.2	78.0	ACIS-S
NGC3379	7076	70.1	65.9	ACIS-S
NGC4278	4741	37.9	34.3	ACIS-S
NGC4278	7077	111.7	101.9	ACIS-S
NGC4278	7078	52.1	45.8	ACIS-S
NGC4278	7079	106.4	99.0	ACIS-S
NGC4278	7080	56.5	52.9	ACIS-S
NGC4278	7081 [†]	112.1	103.6	ACIS-S
NGC4697	784	39.8	37.3	ACIS-S
NGC4697	4727	40.5	36.0	ACIS-S
NGC4697	4728	36.2	30.9	ACIS-S
NGC4697	4729	38.6	19.2	ACIS-S
NGC4697	4730 [†]	40.6	36.5	ACIS-S

[†] The coordinate system of these observations were used as reference when merging observations.

To subtract the background, we use nearby regions on the ACIS-S3 CCD for all galaxies but NGC4697. This can be done since the optical extents of the galaxies does not fill the field-of-view of the ACIS-S3 CCD. For NGC4697 we use extra care in subtracting the background components for two reasons. First, it is located in a galaxy group, and second the galaxy is located in the north polar spur. Therefore, we use the ACIS-S1 CCD to determine the total background component, which is composed of the instrumental background components and the sky background, which includes the soft Galactic emission, the population of unresolved cosmic X-ray background sources, and the emission associated with the north polar spur.

3.2. Two-Micron All Sky Survey

To derive the stellar mass and trace the stellar light of the sample galaxies, we rely on the K-band data of the Two-Micron All Sky Survey (2MASS) Large Galaxy Atlas (LGA) (Jarrett et al. 2003). The K-band images, provided by the 2MASS archive, are background subtracted for all three galaxies except for NGC4278. Therefore, we used nearby regions off NGC4278 to estimate and subtract the background level. The observed background subtracted K-band counts (S) were converted to physical units using

$$m_K = \text{KMAGZP} - 2.5 \log S, \quad (1)$$

where m_K is the apparent K-band magnitude, and KMAGZP is the zero point magnitude given in the image header. For each galaxy we compute m_K using equation (1), which we convert to absolute magnitude and fur-

ther to luminosity, assuming that the absolute K-band magnitude of the Sun is $M_{K,\odot} = 3.28 \text{ mag}$.

The total K-band luminosities of the sample galaxies are very similar, and lie in the range of $(6.1 - 8.2) \times 10^{10} L_{K,\odot}$. Based on the K-band luminosity and the K-band mass-to-light ratios (M_*/L_K) of the galaxies, we compute their total stellar masses. To compute M_*/L_K ratios, we rely on the $B - V$ color indices (de Vaucouleurs et al. 1991) and the results of galaxy evolution modeling (Bell et al. 2003) (Table 1). Since the derived M_*/L_K ratios are very similar in each galaxy, the resulting stellar masses are also compatible and are in the range of $(5.1 - 6.8) \times 10^{10} M_\odot$ (Table 1).

4. THE X-RAY CONTENT OF THE GALAXIES

To unveil whether the sample galaxies host a notable amount of warm X-ray gas, we use three different approaches, discussed throughout this section. First, we compare the surface brightness distribution of the soft (0.3 – 1.2 keV) band unresolved X-ray emission with that of the K-band light. Since the distribution of the faint compact objects follows the stellar light, a deviation from the K-band profile may indicate the presence of warm gas. Second, we compute X-ray-to-K-band luminosity (L_X/L_K) ratios of the unresolved X-ray emission in the 0.5 – 2 keV energy band and compare these with values obtained for admittedly gas-free galaxies and the Milky Way. An L_X/L_K ratio significantly exceeding that of gas-free galaxies will demonstrate the presence of excess X-ray emission, presumably originating from warm X-ray gas. Finally, we extract X-ray energy spectra of the sample galaxies. If warm X-ray gas is present, its physical properties can be measured by spectral fitting.

4.1. X-ray surface brightness profiles

To construct X-ray surface brightness distributions of the unresolved emission, we extracted profiles in the 0.3 – 1.2 keV energy range using circular annuli centered on the centroid of each galaxy. For each profile, detected sources were excluded, a vignetting correction was applied, and the background level was subtracted. The X-ray light distribution is compared with the K-band profiles. To obtain the K-band profiles, the same regions were used, and the same source regions were excluded. The K-band profiles are normalized to approximately match the level of X-ray emission. Although the normalization of the K-band profiles are arbitrary, the particular choice for NGC4278 and NGC4697 was motivated by the spatial distribution of the diffuse X-ray emission, discussed in Section 4.5. The resulting profiles are shown in Figure 2.

Figure 2 demonstrates that in two galaxies, NGC3379 and NGC821, the X-ray light is well traced by the stellar light distribution at all radii. The good agreement between the X-ray and K-band profiles hints that the unresolved X-ray emission in these galaxies has a stellar origin; that is, it originates from the multitude of faint compact objects. However, in NGC4278 and NGC4697, the distribution of the X-ray light shows deviations from the near-infrared profiles. In particular, the unresolved X-ray emission in NGC4278 has a steeper distribution in the central $\sim 35''$ than the stellar light, beyond which radius it follows the K-band profile. Thus, an excess X-ray emitting component is present within the central

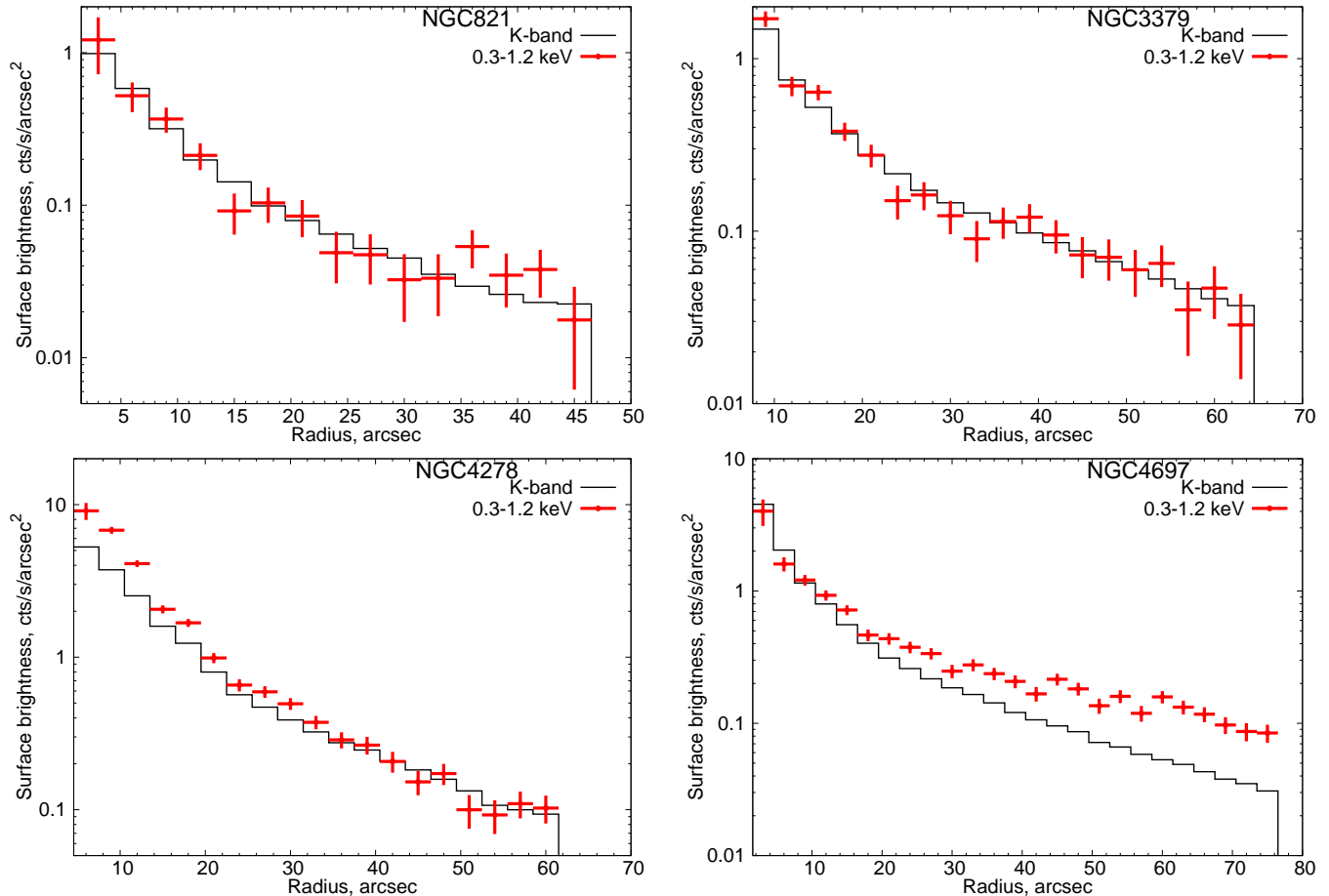


FIG. 2.— Surface brightness distribution of the 0.3 – 1.2 keV band unresolved X-ray emission for the sample galaxies. To construct the profiles we used circular annuli centered on the centroid of each galaxy. Vignetting correction is applied and the background components are subtracted. The X-ray light distribution is compared with the K-band light profiles, which are obtained using the same regions. The K-band profiles are arbitrarily normalized.

regions of NGC4278. In NGC4697 the X-ray light exhibits a significantly broader distribution than the stellar light. This suggests that the bulk of the unresolved soft band X-ray emission arises from the excess X-ray emitting component, which is present at all radii. The nature and properties of the excess X-ray emitting components in NGC4278 and NGC4697 are extensively discussed in the upcoming sections.

4.2. L_X/L_K luminosity ratios

In old stellar populations, the L_X/L_K ratio for the population of faint compact objects is fairly uniform, and is in the range of $L_{0.5-2\text{keV}}/L_K = (3 - 8) \times 10^{27} \text{ erg s}^{-1} L_{K,\odot}^{-1}$ (Sazonov et al. 2006; Revnivtsev et al. 2008; Bogdán & Gilfanov 2011a). By computing the L_X/L_K ratios for the sample galaxies, we can unveil whether the unresolved X-ray emission is dominated by faint compact sources or if other X-ray emitting components also play a role.

To compute the L_X/L_K ratios for each galaxy, we extracted X-ray energy spectra of the D_{25} regions with detected point sources excluded. The spectra were described with a two component model consisting of an optically-thin thermal plasma emission model (APEC in

XSPEC) and a power law model. The abundances were left free to vary, whereas the column density was fixed at the Galactic value (Dickey & Lockman 1990). From the best-fit spectra, we computed the total 0.5 – 2 keV X-ray luminosity, which was used to derive the L_X/L_K ratio for the D_{25} regions.

However, the measured X-ray luminosities do not only reflect the luminosity of the undetected faint compact objects and possible warm X-ray gas, but are also contaminated with two other factors. First, a relatively small fraction ($\lesssim 2\%$) of the detected source counts fall outside the source cells and contribute to the unresolved emission, which must be taken into account. Second, the available *Chandra* exposures do not allow us to resolve all LMXBs. Therefore, the contribution of unresolved LMXBs must also be subtracted. To account for these contaminating factors, we follow the techniques described in Bogdán & Gilfanov (2011a): The residual counts from the detected sources are subtracted on a source-by-source basis, whereas the contribution of unresolved LMXBs is removed using the average LMXB luminosity function (Gilfanov 2004).

The observed and contamination subtracted 0.5 – 2 keV band X-ray luminosities, the K-band luminosity,

TABLE 3
 L_X/L_K RATIOS OBSERVED FOR THE SAMPLE GALAXIES

Galaxy	$L_{0.5-2\text{keV}}$ (erg s^{-1})	$L_{0.5-2\text{keV,XB,sub}}$ (erg s^{-1})	L_K ($L_{K,\odot}$)	$L_{0.5-2\text{keV,XB,sub}}/L_K$ ($\text{erg s}^{-1} L_{K,\odot}^{-1}$)
	(1)	(2)	(3)	(4)
NGC821	2.9×10^{38}	2.8×10^{38}	8.2×10^{10}	3.4×10^{27}
NGC3379	2.4×10^{38}	2.2×10^{38}	6.1×10^{10}	3.6×10^{27}
NGC4278	1.2×10^{39}	1.1×10^{39}	7.1×10^{10}	1.5×10^{28}
NGC4697	2.7×10^{39}	2.6×10^{39}	8.1×10^{10}	3.2×10^{28}
M32 [†]	—	—	—	3.5×10^{27}
Solar neighborhood [‡]	—	—	—	7.7×10^{27}

Note. Columns are as follows. (1) Total observed 0.5 – 2 keV band X-ray luminosity within the D_{25} ellipse after the removal of all detected point sources. The contribution of CXB sources and the contribution of source counts falling outside the source cells has been subtracted. (2) Total observed 0.5 – 2 keV band X-ray luminosity within the D_{25} ellipse after the emission from unresolved LMXBs is subtracted. (3) K-band luminosity of galaxies. (4) Contamination subtracted L_X/L_K ratios in the 0.5 – 2 keV energy range, computed from columns (2) and (3).

[†]Bogdán & Gilfanov (2011a); [‡] Sazonov et al. (2006)

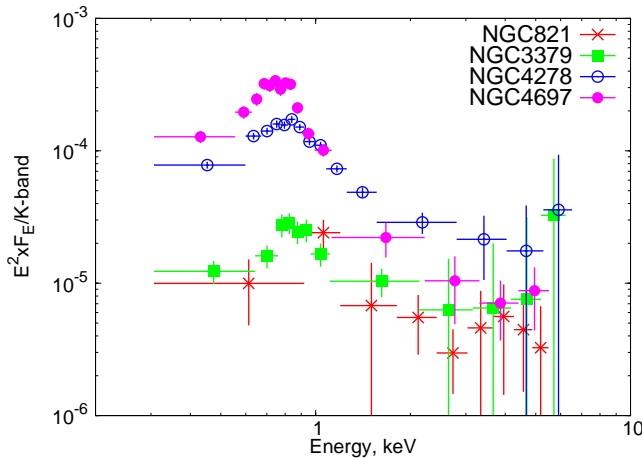


FIG. 3.— X-ray energy spectra of the four studied galaxies obtained for the D_{25} regions. To facilitate comparison, the spectra are normalized to the K-band luminosity of $10^{11} L_{K,\odot}$ and to the distance of 10 Mpc. Bright point sources are excluded and the background components are subtracted.

and the resulting L_X/L_K ratios are listed in Table 3. In the same table we also list the ratios for the gas-free dwarf elliptical galaxy, M32 (Bogdán & Gilfanov 2011a), and the Solar neighborhood (Sazonov et al. 2006). The contamination subtracted L_X/L_K ratios obtained for NGC821 and NGC3379 are in the range of $(3 - 4) \times 10^{27} \text{ erg s}^{-1} L_{K,\odot}^{-1}$, in good agreement with the ratios observed for M32 and for the Solar neighborhood. However, in NGC4278 and NGC4697, we observe $(1.5 - 3.2) \times 10^{28} \text{ erg s}^{-1} L_{K,\odot}^{-1}$, factors of $\sim 4 - 10$ times larger than that obtained for gas-free systems. Thus, based on the L_X/L_K ratios, the unresolved emission in NGC821 and NGC3379 is dominated by the population of faint compact objects, whereas in NGC4278 and NGC4697 an additional X-ray emitting component is present, presumably originating from warm X-ray gas.

4.3. X-ray energy spectra

To confirm the presence of warm X-ray gas in NGC4278 and NGC4697, we extracted their X-ray energy spectra, and compare them to those derived for the gas-free galaxies NGC821 and NGC3379. The spectra, shown in Figure 3, are extracted from within the D_{25} re-

gions. To facilitate the comparison of the observed spectra, we normalize the spectra to the K-band luminosity of $10^{11} L_{K,\odot}$ and the distance of 10 Mpc. Bright point sources are excluded and all background components are subtracted from the depicted spectra.

The spectra demonstrate that NGC4278 and NGC4697 host a prominent soft component at energies $\lesssim 1.5$ keV, whereas such a component is absent in NGC821 and NGC3379. We note that the weak soft component in the spectra of NGC821 and NGC4278 is most likely due to the soft X-ray spectra of active binaries (e.g. Revnivtsev et al. 2006). Above ~ 1.5 keV energy the spectra are in fairly good agreement with each other, which is also confirmed by the 2 – 10 keV band L_X/L_K ratios (Bogdán & Gilfanov 2011a). To study the physical properties of the warm gas, we describe the spectra as a two component model consisting of an optically-thin thermal plasma emission model (APEC in XSPEC) and a power law component. During the fitting procedure the column density was fixed at the Galactic value, whereas the abundance was set free. The thermal plasma emission model gives an acceptable fit for the soft band X-ray spectrum of both galaxies, thereby confirming that the emission originates from warm gas. The best-fit average temperature of the warm gas is $kT = 0.46 \pm 0.02$ keV and $kT = 0.44 \pm 0.03$ keV for NGC4278 and NGC4697, respectively. Thus, the spectra confirm that NGC4278 and NGC4697 host a moderate amount of X-ray emitting gas, while the unresolved X-ray emission in NGC821 and NGC4697 is dominated by the population of faint unresolved sources.

4.4. The X-ray gas content of NGC3379

In NGC3379 we did not detect notable X-ray emission from warm gas, in agreement with the results of Revnivtsev et al. (2008). However, our conclusions are in conflict with those of Trinchieri et al. (2008), who claimed that NGC3379 hosts X-ray emitting gas within the central $< 20''$. In principle, it is possible that the applied point source exclusion regions by Trinchieri et al. (2008) were too small, and the excess emission in the central regions is due to “spill-over” counts from bright point sources. Within the central $20''$ circular region we detect 12809 source counts in the 0.5 – 2 keV band, of which 12491 are associated with bright point sources, if

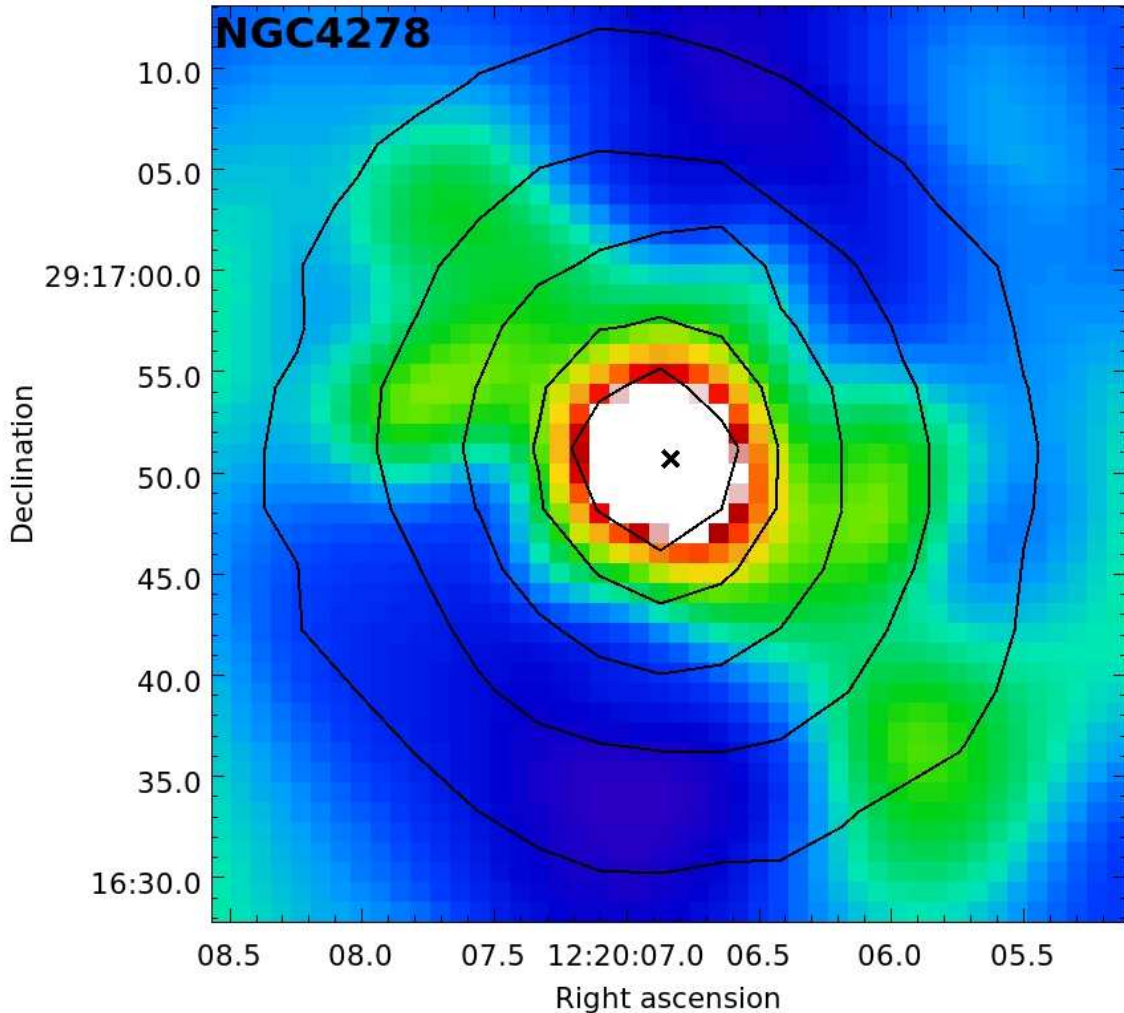


FIG. 4.— X-ray to K-band ratio image for the central $45'' \times 45''$ region of NGC4278. Overplotted contours show the distribution of K-band light and the cross marks the center of the galaxy. The warm X-ray gas extends to at least $\sim 20''$ (~ 1.5 kpc) projected distance and shows an elongated distribution in the northeast-southwest direction, hinting the presence of a galactic-scale outflow. Details on how the image was constructed are discussed in Section 4.5.

$2''$ aperture radii are used as in Trinchieri et al. (2008). That is, only 318 counts, or $\approx 2.5\%$ of the total counts, could be associated with the diffuse emission within the central $20''$ region. Since on-axis the applied $2''$ source aperture encircles $\sim 98\%$ of the point spread function for 0.5 keV energy, the number of “spill-over” counts from point sources is ~ 250 within the central $20''$. Thus, $\sim 79\%$ of the unresolved counts are likely to be associated with bright point sources rather than truly the diffuse emission. Finally, we also mention that $\approx 43\%$ of the source counts originates from the nuclear source in NGC3379, hence the fraction of “spill-over” counts is most significant in the central $\sim 10''$ region. Therefore, to avoid being dominated by the source counts falling outside the source cells, we excluded the central $7''$ of NGC3379 throughout this study.

4.5. Morphology of the warm X-ray gas in NGC4278 and NGC4697

Having demonstrated the presence of warm gas in NGC4278 and NGC4697, we aim to map its morphol-

ogy. Understanding the spatial distribution of the gas may provide important hints about its physical state. We use two techniques to unveil the morphology of the gas. First, we produce a ratio image of the 0.3 – 1.2 keV band X-ray image and the K-band image. The X-ray-to-K-band ratio image allows us to only study the distribution of the warm gas, since other X-ray emitting components – whose luminosity is proportional with the K-band light – are removed. However, this procedure has certain weaknesses: in regions where the X-ray emission is not associated with the K-band light, the ratio image may have very large values; and due to the strongly processed nature of the images, the central few arcsec regions cannot be trusted. To gain insight into the distribution of the warm gas, we prepared both the X-ray and the K-band images. In particular, we excluded the resolved X-ray sources from the 0.5–2 keV band *Chandra* images, and filled their locations with the local emission level applying the DMFILTH task of CIAO. Moreover, the X-ray images are vignetting corrected, the estimated background level is subtracted, and adaptive smoothing

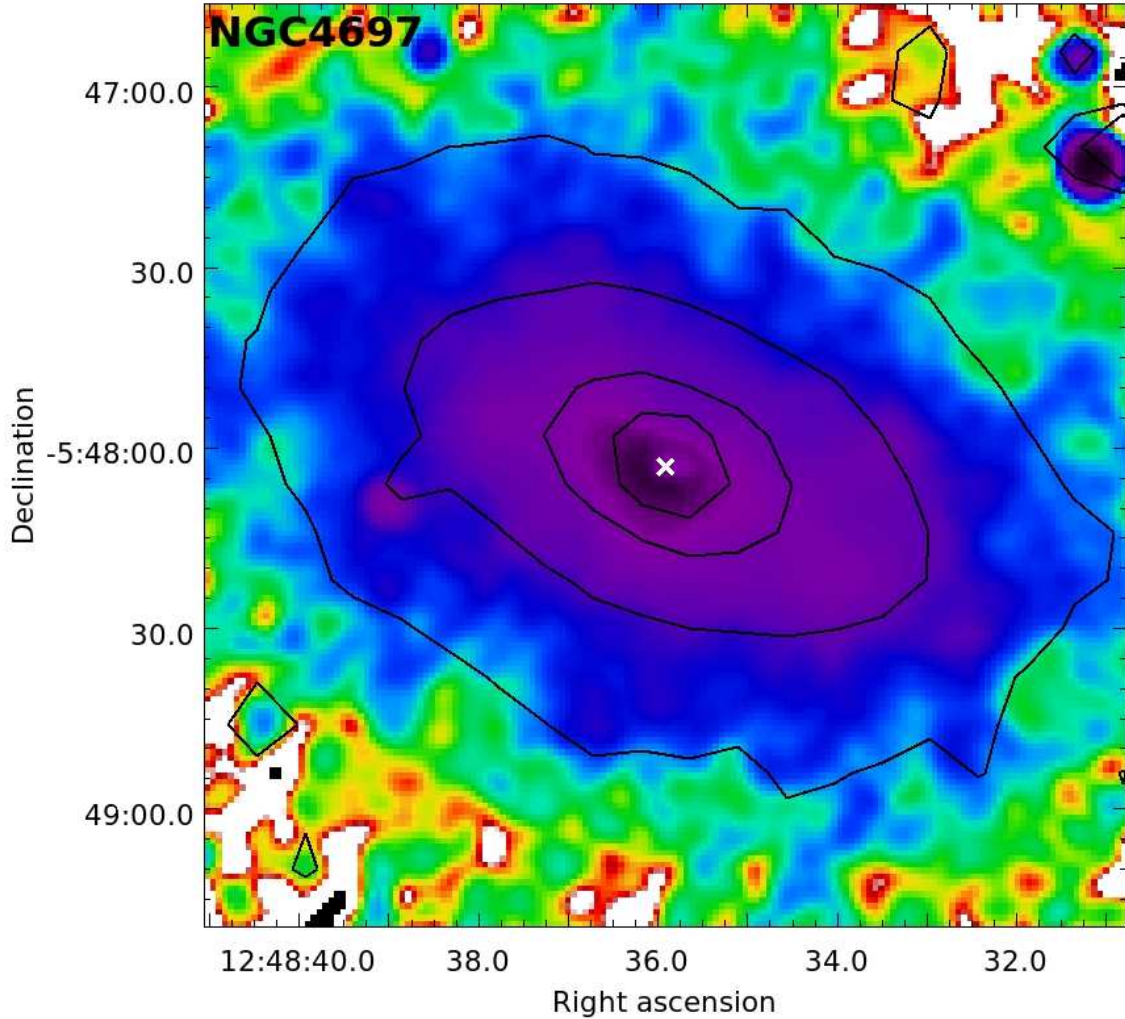


FIG. 5.— X-ray to K-band ratio image for the central $150'' \times 150''$ region of NGC4697. Overplotted contours show the distribution of K-band light and the cross marks the center of the galaxies. The image illustrates that the warm X-ray gas has a notably broader distribution than the stellar light. However, besides its broad distribution, the X-ray gas does not exhibit any further asymmetries. Details on how the image was constructed are discussed in Section 4.5.

is applied using the CIAO `CSMOOTH` tool. The K-band images were smoothed by convolving them with a gaussian. The applied smoothing widths were comparable with the typical smoothing widths near the center of the X-ray images.

The X-ray-to-K-band ratio images for NGC4278 and NGC4697 are depicted in Figure 4 and Figure 5, respectively. For NGC4278 we show the central $45'' \times 45''$ region, where the warm X-ray emitting gas is located. Figure 4 demonstrates that the gas distribution in NGC4278 significantly deviates from the stellar light: the X-ray emission is strongly elongated in the northeast-southwest direction, which may indicate the presence of a galactic-scale outflow. Figure 5 shows the X-ray-to-K-band ratio image for NGC4697. Since the X-ray gas has a broad distribution in NGC4697, we studied the central $150'' \times 150''$ region. We note that $\sim 80\%$ of the stellar light is confined within this region. The ratio image confirms our previous findings, namely that the warm gas is significantly more extended than the stellar light. However, besides

the broad gas distribution, we did not detect any notable asymmetries associated with the gas distribution.

As a second approach we produce X-ray surface brightness distribution profiles of the $0.3 - 1.2$ keV band unresolved emission using circular wedges (Figure 6). The profiles are obtained in the same way as described in Section 4.1. The X-ray profiles are compared with the K-band light distributions, whose normalization agrees with those applied in Figure 2. The major advantage of this method is that we deal with the original X-ray and K-band images, which are not affected by the various processing procedures. Therefore, these profiles can confirm our findings based on the X-ray-to-K-band ratio images. Since the warm gas is centrally concentrated in NGC4278, the inner and outer radii of the applied annulus is $7 - 23''$. The left panel of Figure 6 confirms the elongated distribution of the warm gas: the soft band X-ray emission has two major peaks, namely at the position angles of $105 - 165^\circ$ and $285 - 345^\circ$, which correspond to the northeast and southwest directions. In the right

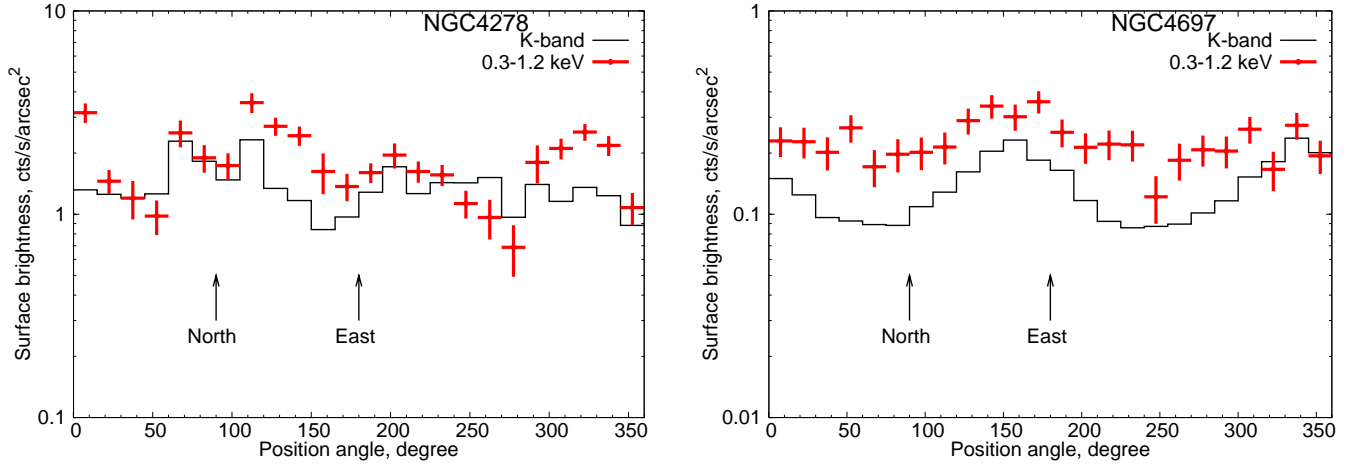


FIG. 6.— Surface brightness distribution of the 0.3 – 1.2 keV energy band unresolved X-ray emission for NGC4278 (left panel) and NGC4697 (right panel). The profiles are obtained for circular wedges, whose inner and outer radii are $7 - 23''$ for NGC4278 and $20 - 50''$ for NGC4697. As shown in the plots, 90° corresponds to north and 180° corresponds to east. Vignetting correction is applied and the background components are subtracted. The X-ray profiles are compared with the K-band profiles. Note that the normalization of the K-band profiles agree with those of Figure 2.

panel of Figure 6 we show the surface brightness profiles for NGC4697, which was obtained for circular annulus with inner and outer radii of $20 - 50''$. As expected from the X-ray-to-K-band image, the X-ray profiles are approximately uniformly higher than the K-band profiles at every position angle. Thus, the profiles do not unveil any major asymmetries associated with the X-ray light distribution.

5. DISCUSSION

5.1. Physical state of the warm gas in NGC4278

The elongated distribution of the warm gas in NGC4278 suggests that it is not in hydrostatic equilibrium, but more likely in an outflow state. In principle, warm gas outflows can be driven by the energy input of SNe Ia and the outflowing mass can be replenished by stellar yields from evolved stars. To understand whether a galactic-scale outflow can be sustained in NGC4278, we investigate the mass and energy budget of the galaxy.

Since the dominant fraction of the warm X-ray gas is located in the central regions of the galaxy, we use two rectangular boxes with $9'' \times 20''$ (0.7×1.56 kpc) that are coincident with the elongated features detected in the X-ray-to-K-band image (Figure 4). For further computations, we assume that the path length of the gas is 0.7 kpc. We extract a combined spectrum from these regions, which also confirms the thermal nature of the emission. The best-fit temperature and abundance of the warm gas is $kT = 0.58 \pm 0.03$ keV and $0.12^{+0.11}_{-0.03}$ Solar (Grevesse & Sauval 1998). The projected temperature profile, obtained from fitting circular annuli centered on the centroid of NGC4278, illustrates that within the central $40''$ region the gas temperature is approximately isothermal with $kT \sim 0.6$ keV (Figure 7 left panel). The $0.5 - 2$ keV X-ray luminosity of the thermal emission in the studied cylindrical shell is 3.2×10^{38} erg s $^{-1}$. From the emission measure, we estimate that the gas mass within the studied volume is $\sim 10^6 M_\odot$, the average number density is 0.05 cm $^{-3}$, and the cooling time is $t_{\text{cool}} = (3kT)/(n_e \Lambda(T)) \approx 1.2 \times 10^8$ years.

Given the parameters of the X-ray gas, we investigate whether the stellar yields from evolved stars can maintain the outflow. The average stellar yield in elliptical galaxies is $\sim 0.0021 (L_K/L_{K,\odot}) M_\odot \text{ Gyr}^{-1}$ (Knapp et al. 1992). The K-band luminosity of the cylindrical shell is $L_K = 6.0 \times 10^9 L_{K,\odot}$, hence the mass loss rate is $\dot{M}_* = 0.013 M_\odot \text{ yr}^{-1}$. Thus, the stellar yields are able to produce the observed gas mass in a timescale of $\sim 8 \times 10^7$ years, which is shorter, but comparable with the cooling time of the gas. The observed low gas mass and the short replenishment time of the gas indicates that the stellar yields from evolved stars are not retained in the galaxy, but are removed in the form of a galactic-scale outflow.

If the gas is outflowing from the galaxy, SNe Ia are likely candidates to drive the outflow. Therefore, we compute whether the energy input from SNe Ia is sufficient to sustain the outflow. The frequency of SNe Ia in old stellar populations, such as NGC4278, is proportional to the stellar mass and hence with the K-band luminosity of the galaxy. Indeed, Mannucci et al. (2005) observed an SN Ia frequency of $N_{\text{SNIa}} = 0.035^{+0.013}_{-0.011}$ SNU for E and S0 galaxies, where 1 SNU = 1 SN/ $10^{10} L_{K,\odot}$ per century. Based on the K-band luminosity of the selected regions, the estimated average SN Ia rate is $2.1 \times 10^{-4} \text{ yr}^{-1}$. Assuming that the average energy output of one SN Ia is 10^{51} erg, we estimate that at most 6.7×10^{39} erg s $^{-1}$ is available to heat the gas and drive the outflow. The required power to drive the outflow can be computed as

$$P_{\text{lift}} = 7.2 \dot{M}_* \sigma^2 \quad (2)$$

where \dot{M}_* is the stellar mass loss rate and σ is the velocity dispersion of the galaxy (David et al. 2006). Using the velocity dispersion of NGC4278 ($\sigma = 237.2$ km s $^{-1}$ – Paturel et al. 2003; HyperLeda²) and the stellar mass-loss rate ($\dot{M}_* = 0.013 M_\odot \text{ yr}^{-1}$), we estimate that $P_{\text{lift}} = 3.3 \times 10^{39}$ erg s $^{-1}$ is needed to drive the outflow. The gas shed by evolved stars is shock heated to the

² <http://leda.univ-lyon1.fr>

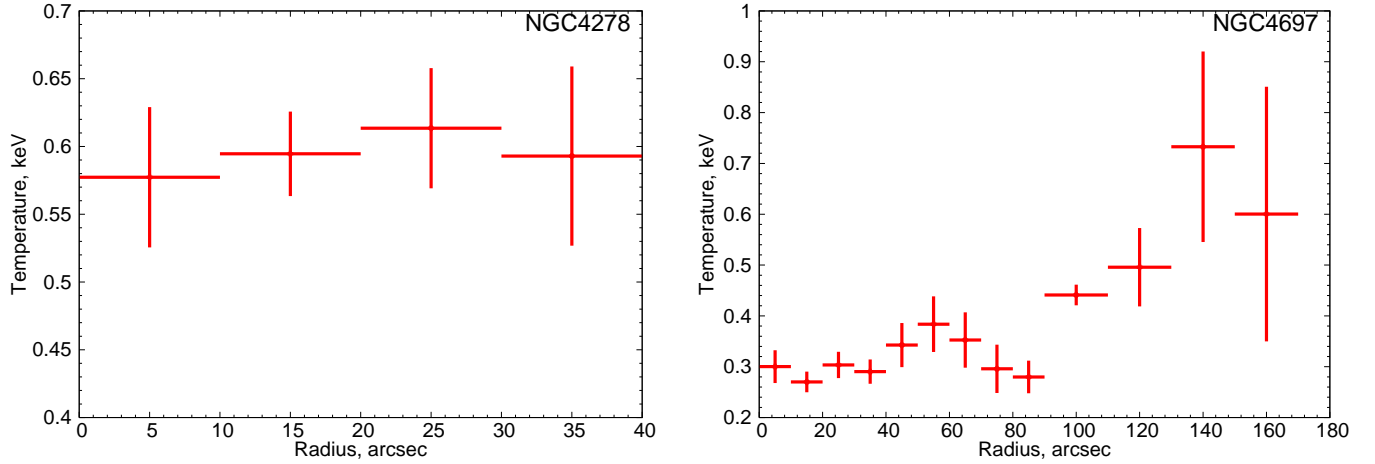


FIG. 7.— Projected temperature profiles of the diffuse emission in NGC4278 (left panel) and NGC4697 (right panel). To obtain the profiles the X-ray energy spectra were extracted from circular annuli centered on the center of the galaxies. The spectra were described with a two component model consisting of a thermal plasma (APEC in Xspec) and a power law model. The depicted temperatures are the best-fit temperatures of the thermal component.

virial temperature of $kT = \sigma^2 \mu m_p = 0.36$ keV, adopting $\mu = 0.62$. Since the observed X-ray gas temperature is ~ 0.6 keV (Figure 7 left panel), SNe Ia need to heat the gas an additional ~ 0.24 keV per particle, which in total requires $\sim 3 \times 10^{38}$ erg s $^{-1}$. Hence, $\sim 4\%$ of the total SN Ia energy is converted to thermal energy, which is consistent with that obtained for spiral galaxies (Mineo et al. 2012). This implies that the total power required to heat the gas and drive the outflow is $P_{\text{tot}} \sim 3.6 \times 10^{39}$ erg s $^{-1}$, which is $\sim 55\%$ of that available from SNe Ia. Thus, we confirm that SNe Ia are capable of sustaining a galactic-scale outflow in NGC4278.

Although the energy input of SNe Ia can sustain a galactic-scale wind, in principle it is possible that the central supermassive black hole also plays a role in driving the outflow. NGC4278 hosts a low-luminosity AGN, which at present is in outburst, exhibiting a parsec scale radio jet (Giroletti et al. 2005). The estimated black hole mass of NGC4278 based on the $M_{\bullet} - \sigma$ relation (Gültekin et al. 2009) and the velocity dispersion of the galaxy ($\sigma = 237.2$ km s $^{-1}$) is $\sim 3.3 \times 10^8 M_{\odot}$. Assuming that the outflow is driven by the energy input of a preceding AGN outburst, we estimate the occurrence time of the presumed outburst. Based on the X-ray surface brightness profile (Figure 2), the outflow may extend to $\sim 35''$ (~ 2.7 kpc). If the gas moves with the sound speed, which in an 0.6 keV plasma is $c_s = \sqrt{(\gamma kT)/(\mu m_H)} \approx 390$ km s $^{-1}$, adopting $\gamma = 5/3$ and $\mu = 0.62$, we derive that the outburst occurred $\sim 7 \times 10^6$ years ago. However, two observational flaws make this proposed interpretation unlikely: First, if an outburst happened $\sim 7 \times 10^6$ years ago, the detection of radio emission associated with the outburst would be likely. However, in the 1.4 GHz Very Large Array (VLA) observation of NGC4278 only the nucleus is detected, but no extended radio emission is observed. Second, AGN outbursts produce X-ray cavities in the warm gas distribution (e.g. Bogdán et al. 2011b). Our *Chandra* images do not reveal such cavities. Instead, the morphology of the X-ray gas is consistent with a bipolar galactic-scale outflow (Figure 4). We thus conclude

that the galactic-scale outflow in NGC4278 is most likely driven by the energy input of the population of SNe Ia.

Based on the detection of an SN Ia driven outflow in NGC4278, we can constrain the supernova efficiency parameter (ξ), which is the percentage of the supernova energy that heats the gas and drives the outflow. Numerical simulations by Thornton et al. (1998) showed that the value of ξ is typically $\sim 10\%$, but may be as high as $\sim 30\%$. The presence of an SN Ia driven outflow in NGC4278 implies that the supernova efficiency parameter is $\xi \gtrsim 55\%$, exceeding those predicted by numerical simulations.

5.2. Physical state of the warm gas in NGC4697

The extended spatial distribution of the warm gas is consistent with two physical states. The warm X-ray gas either may be in hydrostatic equilibrium in the potential well of the galaxy, or it may undergo a subsonic SN Ia driven outflow. To discriminate between these possibilities, we compute the physical properties of the X-ray gas and its mass and energy budget.

To explore the physical properties of the warm X-ray gas in NGC4697, we extract X-ray energy spectra using circular annuli centered on the centroid of the galaxy. We describe the spectra with a two component model, consisting of a thermal plasma emission model (APEC) and a power law model. The abundances of the thermal model are fixed at 0.1 Solar (Grevesse & Sauval 1998) and the column density is fixed at the Galactic value. From the best-fit temperatures of the thermal components, we derive a projected temperature profile, shown in the right panel of Figure 7. The profile demonstrates that within the central $\sim 90''$ the X-ray gas is approximately isothermal with $kT \sim 0.3$ – 0.4 keV, beyond which radius the X-ray gas temperature gradually increases to $kT \sim 0.7$ keV. This result can be interpreted in a simple manner in view of the environment of NGC4697. Indeed, NGC4697 is a member of a small galaxy group with 10 members, hence the gas with ~ 0.7 keV temperature is most likely associated with a larger scale group atmosphere. Thus, within the central $\sim 90''$ radius the

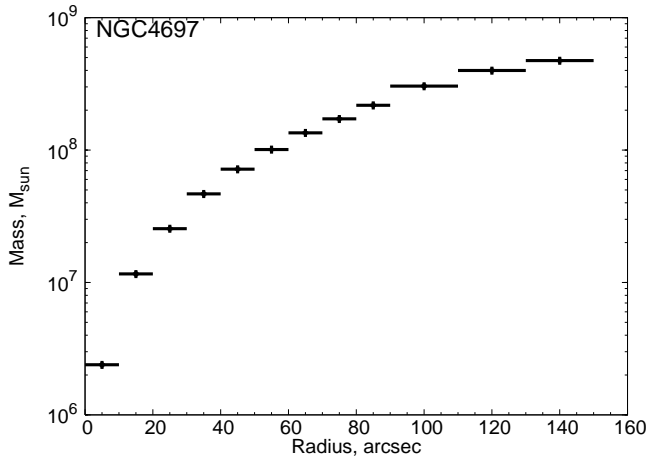


FIG. 8.— Cumulative gas mass distribution for NGC4697. To obtain the gas mass profile, spherical symmetric gas distribution was assumed. The total stellar mass within $90''$ is $5.4 \times 10^{10} M_{\odot}$, implying an X-ray gas mass fraction of $\sim 0.4\%$.

$\sim 0.3 - 0.4$ keV galaxy gas dominates the diffuse emission, and at larger radii the hotter group gas becomes predominant.

We derive the X-ray gas mass by employing the same spectral extraction regions, and assuming a spherically symmetric gas distribution. From the emission measure of the thermal component, we derive the confined gas mass in each shell. The resulting cumulative mass profile is depicted in Figure 8, which shows that within $90''$, NGC4697 contains $\sim 2.2 \times 10^8 M_{\odot}$ of gas. We note that this region comprises $\sim 82\%$ of the total stellar light of the galaxy. The total stellar mass within $90''$ is $5.4 \times 10^{10} M_{\odot}$, hence the X-ray gas mass fraction is $\sim 0.4\%$, which significantly exceeds that of NGC4278 ($\sim 0.02\%$ – Section 5.1), and is consistent with values obtained for more X-ray luminous galaxies ($\sim 1\%$ – Fukazawa et al. 2006), whose X-ray gas content is in hydrostatic equilibrium. This suggests that the X-ray gas content of NGC4697 is in hydrostatic equilibrium rather than in an outflow state.

To further study the physical state of the gas, we derive the time scale, on which the observed gas can be replenished by the stellar yields of evolved stars. Since the galaxy gas dominates the X-ray emission within $\sim 90''$ radius, the calculations presented below refer to this region. Using the average stellar yields for elliptical galaxies (Knapp et al. 1992), we estimate an average mass loss rate of $0.14 M_{\odot} \text{ yr}^{-1}$. Hence, evolved stars can replenish the observed $\sim 2.2 \times 10^8 M_{\odot}$ X-ray gas mass on a time scale of ~ 1.6 Gyrs. This time scale exceeds the cooling time, which is $\lesssim 1$ Gyr within the central $\sim 90''$ region. Thus, most, if not all warm X-ray gas has been retained in hydrostatic equilibrium in the past ~ 1.6 Gyrs, implying the absence of galactic-scale outflows.

Alternatively, it is also feasible that only a fraction of the X-ray gas leaves the galaxy in a subsonic outflow driven by the energy input of SNe Ia (David et al. 1991). We derive the available energy input from SNe Ia, using the average SN Ia frequency in E/S0 galaxies (Mannucci et al. 2005) and the K-band luminosity of NGC4697. We obtain an SN Ia rate of $2.3 \times 10^{-3} \text{ yr}^{-1}$. Assuming that the average energy output from SNe Ia is 10^{51} erg, SNe Ia can add at most $7.3 \times 10^{40} \text{ erg s}^{-1}$. To estimate the required power to drive the outflow, we use

the velocity dispersion of NGC4697 ($\sigma = 170.9 \text{ km s}^{-1}$ – Paturel et al. 2003; HyperLeda³), the stellar mass-loss rate ($\dot{M}_{\star} = 0.14 M_{\odot} \text{ yr}^{-1}$), and equation (2). We thus obtain $P_{\text{lift}} = 1.9 \times 10^{40} \text{ erg s}^{-1}$. If the gas is heated to the virial temperature of $kT = 0.19$ keV, SNe Ia need to contribute with an additional ~ 0.2 keV per particle, which in total corresponds to $\sim 2 \times 10^{39} \text{ erg s}^{-1}$. Hence, the total required power to heat the gas and drive an outflow is $\sim 2.1 \times 10^{40} \text{ erg s}^{-1}$, which is $\sim 30\%$ of that available from SNe Ia.

Although SNe Ia are energetically capable of driving an outflow, the above-discussed characteristics of the gas indicate the absence of a global galactic-scale outflow. A likely explanation of the absence of an outflow and the large gas mass may be that NGC4697 is located in a galaxy group. Indeed, the temperature profile of the warm X-ray gas demonstrated the presence of hotter component beyond $\sim 90''$ radius, which presumably is associated with the group emission. The warm X-ray gas inside and outside the optical extent is in pressure equilibrium, thereby suggesting that it is in hydrostatic equilibrium and not in an outflow state. This result is in good agreement with those obtained by David et al. (2006), who also concluded that the ambient pressure in a dense environment may be able to suppress the evolution of an outflow.

5.3. Galactic-scale outflows in NGC821 and NGC3379

Although no warm gas is detected from NGC821 and NGC3379, this does not imply the absence of X-ray gas and galactic-scale outflows. As discussed above, evolved stars eject stellar yields at a constant rate, which is proportional with the K-band luminosity (or stellar mass) of the galaxy. Based on the K-band luminosity of NGC821 and NGC3379 and using Knapp et al. (1992), we estimate a mass input rate of $0.17 M_{\odot} \text{ yr}^{-1}$ and $0.13 M_{\odot} \text{ yr}^{-1}$, respectively. Hence, on a timescale of 5 Gyrs, which is comparable with the stellar age of these galaxies (Sánchez-Blázquez et al. 2006), the cumulated gas mass should be on the order of $\sim 10^9 M_{\odot}$. Such large gas masses would imply a gas mass fraction of $\sim 1\%$, similar to those observed in massive, X-ray luminous early-type galaxies (Fukazawa et al. 2006). However, such a large gas mass is not observed in NGC821 and NGC3379, implying that the X-ray gas is driven away from the galaxies.

A plausible way to remove the X-ray gas from the potential well of the sample galaxies is via galactic-scale outflows. To derive whether SNe Ia are energetically capable of driving an outflow, we compute the available energy input from SNe Ia. Given the K-band luminosities of NGC821 and NGC3379 (Table 2) and the average SN Ia frequencies (Mannucci et al. 2005), we obtain SN Ia rates of $2.9 \times 10^{-3} \text{ yr}^{-1}$ and $2.1 \times 10^{-3} \text{ yr}^{-1}$, respectively. Assuming that each SN Ia contributes with $E_{\text{SNIa}} = 10^{51}$ erg energy, we derive that at most $9.2 \times 10^{40} \text{ erg s}^{-1}$ and $6.7 \times 10^{40} \text{ erg s}^{-1}$ is available in NGC821 and NGC3379, respectively. We confront this value with that required to drive the outflow. Therefore, we use equation (2), the stellar mass input rates, and the velocity dispersions of NGC821 and NGC3379, which are 200.2 km s^{-1} and

³ <http://leda.univ-lyon1.fr>

209.2 km s⁻¹, respectively. Hence, to drive an outflow from NGC821 and NGC3379, $P_{\text{lift}} = 3.1 \times 10^{40}$ erg s⁻¹ and $P_{\text{lift}} = 2.6 \times 10^{40}$ erg s⁻¹ is required. Thus, the required power is $\lesssim 40\%$ of that available from SNe Ia, implying that SNe Ia can drive galactic-scale outflows in both galaxies.

The non-detection of X-ray gas in NGC821 and NGC3379, may be explained by the low gas densities. Since the emission measure is proportional to the density square of the gas, the density plays a crucial role in determining the observed X-ray luminosity of the gas. For example, if the gas density in NGC4278 was factor of 3 lower, the X-ray luminosity would decrease by factor of 9. However, such a low luminosity gaseous emission could not be identified, therefore NGC4278 would appear as a gas-free galaxy. Following this line of arguments, it is likely that both NGC821 and NGC3379 host a small amount of outflowing X-ray gas, which remains unidentified due to its relatively low density hence low X-ray luminosity. These considerations are in good agreement with the hydrodynamical simulations of Pellegrini et al. (2007), who showed that the luminosity of an outflow from NGC821 may fall below the detection limit.

5.4. Metallicity of the warm X-ray gas

SNe Ia do not only deposit energy into the X-ray emitting gas, but also enrich it with iron-peak elements. On average, each SN Ia produces 0.7 M_⊙ iron, thereby enriching the interstellar medium. Although the abundance of the stellar ejecta is likely to be sub-solar in low-mass ellipticals (Gallazzi et al. 2006), if the stellar yields undergo complete mixing with the iron-peak elements, the abundances of the warm gas are not expected to agree with the stellar yields, but should be highly super-solar (David et al. 2006; Bogdán & Gilfanov 2008). However, the measured abundances in NGC4278 and NGC4697 are $0.12^{+0.11}_{-0.03}$ and $0.17^{+0.13}_{-0.04}$ (Grevesse & Sauval 1998). That is, both galaxies exhibit strongly sub-solar abundances, in conflict with the theoretical expectations.

The observed low abundances may partly be caused by the modest energy resolution of *Chandra* CCDs and the relatively low number of detected photons, which may result in large systematic uncertainties in the abundance determination. In principle, the problem of inaccurate spectral modelling can be circumvented with the application of grating spectroscopy. Although distant galaxies with very low X-ray gas content are not suitable for such an investigation due to the low number of photons, studies of nearby and/or gas-rich galaxies found that abundances observed from CCD spectra are in fairly good agreement with those observed by grating spectroscopy (Liu et al. 2010; Ji et al. 2009). Therefore, it seems unlikely that the approximately order of magnitude difference between observed and expected abundances originates from systematic uncertainties.

The predicted super-solar abundances invoke the complete mixing of iron with the stellar yields. However, numerical simulations point out that in the case of an outflow, the iron is not well mixed with the ambient gas, resulting in sub-solar abundances (Tang et al. 2009). Therefore, the low abundances observed in NGC4278 (and possibly in NGC4697) may imply that the observed sub-solar abundances are (at least partly) due to the incomplete mixing of stellar yields and iron from SNe Ia.

In general, the low abundance in low-mass ellipticals may be due to the shallow gravitational potential well of these galaxies. At early epochs of galaxy formation, core collapse supernovae produce α -elements. Due to supernova driven winds, a large fraction of these elements could be removed from galaxies with shallow potential wells, but are retained in galaxies with more extended halos (Tremonti et al. 2004; Gallazzi et al. 2006). At later epochs SNe Ia contribute with iron peak elements, thereby enriching the interstellar medium. In general, low-mass ellipticals are more sensitive to AGN and SNe Ia driven outflows at all times, which may have a major influence on its metal enrichment history.

It is also possible that the observed low abundances are in part caused by the iron bias, which appears if a multi-temperature plasma or a temperature gradient is described with a single-temperature model (Buote et al. 2000; Baldi et al. 2006). To illustrate the importance of the iron bias, we produced a set of two-temperature thermal emission model (APEC) spectra for NGC4697, which we fit with a single-temperature model. The temperatures of the model spectra were $kT_1 = 0.2$ keV and $kT_2 = 0.4$ keV, whereas the applied set of abundances varied from 0.2 to 5 Solar (Grevesse & Sauval 1998). The normalizations of the two thermal components were set, and the column density was fixed at the Galactic value. When describing the two-temperature model with a single temperature spectrum, the best-fit temperature – independently from the abundance – is $kT \approx 0.3$ keV. However, the best-fit abundance is significantly lower than the originally assumed value, and it is in all cases sub-solar. In particular, if the original abundances are set to 5/1/0.5 Solar, the best-fit values are $\approx 0.55/0.35/0.25$ Solar. Although all these values exceed that obtained for NGC4697, this examination illustrates that describing a multi-temperature plasma with an overly simplistic spectral model may have major effects on the observed abundances. We stress that this conclusion does not only refer to NGC4697 but is representative for other galaxies with similar parameters as well.

Finally, we mention the existence of a strong degeneracy between the emission measure and the abundance of the warm gas (e.g. David et al. 2006). This degeneracy may have important consequences on the observed parameters of the warm X-ray gas. If, for example, the abundance of the gas is about Solar (~ 10 times higher than the best-fit values for NGC4278 and NGC4697), the derived the gas densities, gas masses, replenishment times, and cooling times must reduced by a factor of ≈ 3.3 .

6. CONCLUSIONS

We studied the unresolved X-ray emission, the warm gas content, and the physical state of the warm X-ray gas in four low-mass elliptical galaxies (NGC821, NGC3379, NGC4278, NGC4697) based on archival *Chandra* observations. Our results can be summarized as follows:

1. We find that the bulk of the unresolved emission in NGC821 and NGC3379 originates from a large number of faint compact objects, such as CVs and ABs. Despite the non-detection of warm gas, low density, hence low luminosity X-ray gas components may be present, which,

driven by the energy input of SNe Ia, outflow from the galaxies at a steady rate.

2. We detect hot X-ray gas in the central $\sim 35''$ (~ 2.8 kpc) region of NGC4278. The temperature of the gas is $kT \sim 0.6$ keV. The warm X-ray gas exhibits a bipolar morphology in the northeast-southwest direction, suggesting that it is outflowing from the galaxy. We conclude that the outflowing mass can be replenished by the stellar yields of evolved stars and the outflow can be driven by the energy input of SNe Ia. Based on the existence of an outflow in NGC4278 and the energy budget of the galaxy, we place a lower limit of $\sim 55\%$ on the supernova efficiency parameter.

3. We show that NGC4697 hosts X-ray gas at all radii, whose temperature within a region with $\sim 90''$ radius is $kT \sim 0.3 - 0.4$ keV, beyond which radius the gas temperature increases to ~ 0.7 keV. We identify the hotter gas with the group atmosphere surrounding NGC4697. Although the X-ray gas has a significantly broader distribution than the stellar light, it does not show any asymmetries. The gas mass within the central $\sim 90''$ region is $\sim 2.2 \times 10^8 M_\odot$, implying a gas mass fraction of $\sim 0.4\%$, which is comparable with those observed in luminous massive early-type galaxies. These evidences

together indicate that the X-ray gas is most likely in hydrostatic equilibrium, however a subsonic outflow cannot be excluded.

Acknowledgements. ÁB thanks Alexey Vikhlinin, Marat Gilfanov, and Junfeng Wang for helpful discussions. This research has made use of *Chandra* data provided by the Chandra X-ray Center. The publication makes use of software provided by the Chandra X-ray Center (CXC) in the application package CIAO. This publication makes use of data products from the Two Micron All Sky Survey, which is a joint project of the University of Massachusetts and the Infrared Processing and Analysis Center/California Institute of Technology, funded by the National Aeronautics and Space Administration and the National Science Foundation. In this work the NASA/IPAC Extragalactic Database (NED) have been used. The authors acknowledge the usage of the HyperLeda database (<http://leda.univ-lyon1.fr>). ÁB acknowledges support provided by NASA through Einstein Postdoctoral Fellowship grant number PF1-120081 awarded by the Chandra X-ray Center, which is operated by the Smithsonian Astrophysical Observatory for NASA under contract NAS8-03060. WF and CJ acknowledge support from the Smithsonian Institution.

REFERENCES

- Baldi, A., Raymond, J. C., Fabbiano, G., et al., 2006, *ApJ*, 162, 113
- Bell, E. F., McIntosh, D. H., Katz, N. & Weinberg, M. D., 2003, *ApJS*, 149, 289
- Bogdán, Á., Gilfanov, M., 2008, *MNRAS*, 388, 56
- Bogdán, Á., Gilfanov, M., 2011a, *MNRAS*, 418, 1901
- Bogdán, Á., Kraft, R. P., Forman, W. R., et al., 2011b, *ApJ*, 743, 59
- Buote, D. A., 2000, *MNRAS*, 311, 176
- Cappellari, M., Emsellem, E., Krajnović, D., et al., 2011, *MNRAS*, 413, 813
- David, L. P., Forman, W. & Jones, C., 1991, *ApJ*, 380, 39
- David, L. P., Jones, C., Forman, W. & Murray, S. S., 2005, *ApJ*, 635, 1053
- David, L. P., Jones, C., Forman, W., Vargas, I. M. & Nulsen, P., 2006, *ApJ*, 653, 207
- de Vaucouleurs, G., et al., Third Reference Catalogue of Bright Galaxies. Springer-Verlag. (1991)
- Dickey, J. M. & Lockman, F. J., 1990, *ARA&A*, 28, 215
- Forman, W., Jones, C. & Tucker, W., 1985, *ApJ*, 293, 102
- Forman, W., Jones, C., Churazov, E., et al., 2007, *ApJ*, 665, 1057
- Fukazawa, Y., Botoya-Nones, J. G., Pu, J., Ohto, A. & Kawano, N., 2006, *ApJ*, 636, 698
- Gallazzi, A., Charlot, S., Brinchmann, J. & White, S. D. M., 2006, *MNRAS*, 370, 1106
- Gilfanov, M., 2004, *MNRAS*, 349, 146
- Gioletti, M., Taylor, G. B. & Giovannini, G., 2005, *ApJ*, 622, 178
- Grevesse, N. & Sauval, A. J., 1998, *SSRv*, 85, 161
- Gültekin, K., Richstone, D. O., Gebhardt, K., et al., 2009, *ApJ*, 698, 198
- Hickox, R. C. & Markevitch, M., 2006, *ApJ*, 645, 95
- Irwin, J. A., Athey, A. E. & Bregman, J. N., 2003, *ApJ*, 587, 356
- Jarrett, T. H., Chester, T., Cutri, R., et al., 2003, *AJ*, 125, 525
- Jensen, J. B., Tonry, J. L., Barris, B. J., et al. 2003, *ApJ*, 583, 712
- Ji, J., Irwin, J. A., Athey, A., Bregman, J. N. & Lloyd-Davies, E. J., 2009, *ApJ*, 696, 2252
- Kim, D.-W., Fabbiano, G., Kalogera, V., et al., 2006, *ApJ*, 652, 1090
- Knapp, G. R., Gunn, J. E. & Wynn-Williams, C. G., 1992, *ApJ*, 399, 76
- Kraft, R. P., Forman, W. R., Jones, C., et al., 2011, *ApJ*, 727, 41
- Li, Z. & Wang, Q. D., 2007, *ApJ*, 668, L39
- Li, Z., Jones, C., Forman, W. R., et al., 2011, *ApJ*, 730, 84
- Liu, J., Wang, Q. D., Li, Z., & Peterson, J. R., 2010, *MNRAS*, 404, 1879
- Mannucci, F., Della Valle, M., Panagia, N., et al., 2005, *A&A*, 433, 807
- Mathews, W. G., Brighenti, F. 2003, *ARA&A*, 41, 191
- Mineo, S., Gilfanov, M. & Sunyaev, R., *MNRAS*, submitted, arXiv:1205.3715
- Moretti, A., Campana, S., Lazzati, D. & Tagliaferri, G., 2003, *ApJ*, 588, 696
- Paturel, G., Petit, C., Prugniel, P., et al., 2003, *A&A*, 412, 45
- Pellegrini, S., Baldi, A., Kim, et al., & Elvis, M., 2007, *ApJ*, 667, 731
- Randall, S. W., Sarazin, C. L. & Irwin, J. A., 2006, *ApJ*, 636, 200
- Revnivtsev, M., Sazonov, S., Gilfanov, M., Churazov, E. & Sunyaev, R., 2006, *A&A*, 452, 169, 178
- Revnivtsev, M., Churazov, E., Sazonov, S., Forman, W. & Jones, C., 2008, *A&A*, 490, 37
- Revnivtsev, M., Sazonov, S., Churazov, E., et al., 2009, *Nature*, 458, 1142
- Sánchez-Blázquez, P., Gorgas, J., Cardiel, N. & González, J. J., 2006, *A&A*, 457, 809
- Sarazin, C. L., Irwin, J. A. & Bregman, J. N., 2001, *ApJ*, 556, 533
- Sazonov, S., Revnivtsev, M., Gilfanov, M., Churazov, E. & Sunyaev, R., 2006, *A&A*, 450, 117
- Tang, S., Wang, Q. D., Mac Low, M.-M. & Joung, M. R., 2009, *MNRAS*, 398, 1468
- Terlevich, A. I. & Forbes, D. A., 2002, *MNRAS*, 330, 547
- Thornton, K., Gaudlitz, M., Janka, H.-Th. & Steinmetz, M., 1998, *ApJ*, 500, 95
- Tremonti, C. A., Heckman, T. M., Kauffmann, G., et al., 2004, *ApJ*, 613, 898
- Trinchieri, G., Pellegrini, S., Fabbiano, G., et al., 2008, *ApJ*, 688, 1000
- Tonry, J. L., Dressler, A., Blakeslee, J. P., et al., C. B., 2001, *ApJ*, 546, 681